Available online at www.sciencedirect.com

ScienceDirect

Transportation Research Procedia 00 (2018) 000–000

Transportation Research Procedia

www.elsevier.com/locate/procedia

World Conference on Transport Research - WCTR 2019 Mumbai 26-31 May 2019--

Design and Analysis of an Experimental Setup for Determining Transfer Length of BFRP Prestressed Beams

Prashant Motwani[a*], Arghadeep Laskar[b]

[a*]*Research Scholar, Indian Institute of Technology Bombay, Mumbai, 400076, India*
[b]*Assitant Professor, Indian Institute of Technology Bombay, Mumbai, 400076, India*

Abstract

This work is a vital step in enhancing the potential use of a newly developed organic Basalt Fiber Reinforced Polymer (BFRP) rebar for prestressed applications in infrastructure projects including bridges, buildings etc. The work investigates the feasibility of BFRP rebars as prestressing strand in lieu of conventional steel prestressing strand and an associated test procedure to determine its transfer length and end slip. An experimental test setup has been designed using nonlinear finite element method to stress and release BFRP strands to transfer prestress in concrete members eliminating use of any special stressing devices and procedures. Prior to the fabrication of the test setup, the details of the configuration of the setup has been designed by conducting a parametric study on the simulated test setup in nonlinear finite element tool ABAQUS. Several parameters like the size of members to be used, orientation of the sections and size and location of stiffener plates have been thoroughly investigated and a robust test setup has been established. The setup later will be utilized to perform pilot tests on BFRP strands at the Indian Institute of Technology, Bombay.

Peer-review under responsibility of WORLD CONFERENCE ON TRANSPORT RESEARCH SOCIETY.

Keywords: ABAQUS, Basalt Fiber Reinforced Polymer, Transfer Length, Nonlinear Finite Element Method

1. Introduction

PC members degrade rapidly when the steel strands are subjected to corrosion thereby decreasing the lifespan of the PC structures. Two major bridge girder collapses in the past has been related to corrosion of prestressing steel; namely the failure of the viaduct “S. Stefano” in Italy in the year 1999 [Colajanni et al. (2016)] and Lowe’s Motor Speedway footbridge in USA in 2000 [Poston and West (2005)].

The maintenance of steel (to prevent it from corrosion) and replacement of the assets (which are affected by corrosion) in a short span of time has become a major problem for an economy. Therefore, it is imperative that corrosion is dealt with utmost priority so that the full effect of the growth may be felt in the economy. Another problem with the use of steel strands is the loss of prestressing force which can go up to 24% for conventionally prestressed members [Gamble et al. (1976)]. Due to this there has been considerable research in last one decade to replace steel strands in prestress members with Fiber Reinforced Polymer (FRP) strands. Aramid and carbon are the most widely accepted FRP strands for construction practices. However both these materials have their own demerits. The major problem with AFRP is that they are sensitive to sunlight and high UV environment. Although CFRP is safe to UV exposure, it exhibits high electrical conductivity.

* Prashant Motwani. Tel.: +91-998113-5555.
E-mail address: pmotwani@iitb.ac.in.

Peer-review under responsibility of WORLD CONFERENCE ON TRANSPORT RESEARCH SOCIETY

Basalt Fiber Reinforced Polymer (BFRP) is a newly developed organic polymer with high resistance to UV exposure, low thermal and electrical conductivity, and high resistance to chemical attack and have a great potential application as a composite material. Overall, the manufacturing process of basalt fibers is similar to glass fibers, but with less energy consumption. Using a natural volcanic basalt rock as raw material, basalt fibers are produced by putting raw materials into a furnace where it is melted at 1450 ºC to 1500 ºC. After this, the molten material is forced through a platinum/rhodium crucible bushings to create fibers. This technology, named continuous spinning, can offer the reinforcement material in the form of chopped or continuous fibers that can be used in various industries like, infrastructure, textile, automobile, etc. In addition to the ability to be easily processed using conventional processes and equipment, the basalt fibers do not contain any other additives in the entire producing process, which makes it economical compared to other FRP [Thorhallsson and Snaebjornsson (2013)]. The comparative material properties of few FRP rebars with steel has been reported by Belarbi et al. (2017) and are shown in Table 1.

Table 1. Mechanical Properties of FRP rebars with Steel [Belarbi et al. 2017].

Property	Steel	BFRP RockBar™	AFRP Arapree™	CFRP CFCC™
Longitudinal Tensile Strength (GPa)	1.86	1.3	1.2-1.5	1.8-2.1
Longitudinal Modulus (GPa)	196	64	62-64	137
Transverse Modulus (GPa)	196	---	5.5	10.3
Elongation (%)	1.5-3	1.6-3.0	0.5-1.9	1.9-4.4
Major Poisson's Ratio	0.30	0.26	0.38	0.27
Minor Poisson's Ratio	0.30	---	0.02	0.02

"---" Indicates that the information is not available with the manufacturer

2. Literature Review

Even though the general information related to FRP reinforcement as internal prestressing strands in concrete is available in ACI 440R-96 (1996), the design procedures for pre-stressed concrete elements using BFRP rebars have not been specified in any design code. Wu et al. (2009) tested BFRP rebars and reported high rupture strength (f_{pu}) from 950 MPa to 2000 MPa, and a relatively low elastic modulus (E_p), ranging from 45 GPa to 65 GPa and concluded that since the strength of BFRP rebars are comparable to steel prestressing strand, while having an elastic modulus four times smaller and weight three times lighter, it can be an alternative to steel prestressing strand for prestressed concrete applications. Another governing factor for BFRP to be utilized as prestressing strand is the lower relaxation loss in these strends. Systematic research on relaxation behaviour of BFRP by Shi et al. (2015), CFRP and AFRP by Saadatmanesh and Tannous (1999a and b) has showed that the relaxation losses for BFRP, CFRP and AFRP were 4.2%, 5.87% and 10.9% , respectively, after a period of 50 years under stress value of 0.4 f_{pu}. This indicates that the pre-stressing loss due to relaxation occurring in pre-stressed concrete elements is comparatively lower in BFRP prestressed members as compared to CFRP and AFRP.

The very low ratio of lateral to axial tensile strength of BFRP rebar makes it impractical to use the conventional steel wedges and barrels for prestressing operation. This is because the low efficiency of the clamping mechanism creates strong concentration of transverse stresses in the rebar and causes it to fail even before reaching its maximum tensile capacity. Several methods for prestressing BFRP strands have been attempted by many researchers to assure the performance of the tensile strength of BFRP strands and are explained below.

- Jacking against External Reaction Frames.

In this method, FRP reinforcement is anchored to an external reaction frame using a binding material. After the binding material has hardened FRP rebar is released from external reaction frame and prestress force is transferred to the RC element. Thorhallsson and Gudmundsson (2013) adopted a similar methodology and utilized chemical anchors, designed for stressing BFRP strands, developed at Reykjavik University. The BFRP strands were glued in to a steel tube with concrete glue and then the assembly was inserted into threaded steel rods. The strands were locked at each end using external end blocks and the prestress was released by cutting the strands.

- Using Internal Thread Type Couplers.

In this method, the FRP rebar is connected to the steel prestressing strand using couplers and the conventional steel wedge and barrel system is utilized for stretching the steel strands. Atutis et al. (2018) tested twelve beams prestressed by BFRP reinforcement, commercially known as RockBar™ composite. The beams were 3.2 meter long and rectangular in cross section with 150 mm

width and 300 mm height. The BFRP rebars were tensioned using special couplers with internal threads, where ends of the BFRP rebar was anchored to steel prestressing strand.

- Using Mechanical Anchors.

In this method, FRP rebar is directly prestressed by pulling anchor at one end while the other end is fixed and this system is analogous to conventional steel prestressing system. Younes et al. (2017) stressed the BFRP bars using a prestressing system having a mechanical anchor. In order to distribute the stresses on the surface of the bar and prevent the wedges from notching the bar, copper sleeves were placed on the bar and then three steel wedges were pushed firmly into the barrel of the grip after they were assembled around the sleeve. Younes et al. (2017) reported that, the load deflection response for BFRP prestressed beams were significantly different from those calculated using provisions in ACI 440R -96 (1996).

Based on the above literature, it can be understood that in order to utilize the full potential of BFRP rebars as prestressing strands it is essential that the strands are stretched without causing any significant stress concentration between the grip and BFRP strands. Therefore, this study aims to develop a test setup using nonlinear finite element method in order to stretch and release BFRP strands by jacking it on external frames and thereby eliminating use of any special stressing devices and procedures.

3. Experimental Setup

The experimental setup has been designed based on the availability of resources at the Indian Institute of Technology, Bombay. A schematic view of the experimental setup is shown in Fig. 1a. A back supporting beam of length 1.1 m and a mid-supporting beam of length 3 m would be fabricated would be fabricated using ISMB-450 rolled section and connected to each other in T-shape (Fig. 1a). A spandrel beam consisting of a built up section would be fabricated using two ISMB-150 section and 8mm rectangular plates (Fig. 1b). Two steel formworks would be fabricated to cast concrete beams of dimensions 100 mm X 200 mm X 3000 mm. Prior to the casting of concrete, 8 mm diameter BFRP strands would be placed inside the steel formworks. The strands would be passed through 15 mm diameter holes drilled on the back supporting beam and the spandrel beam and locked on to these beams using bond type anchors at the two ends, as shown in Fig. 1b and Fig. 1c.

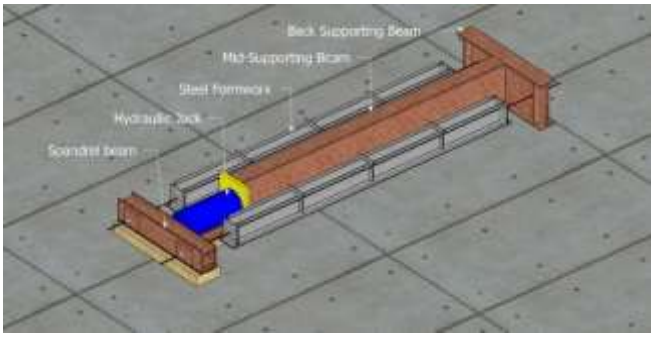

(a) Three Dimensional View of the Experimental Setup

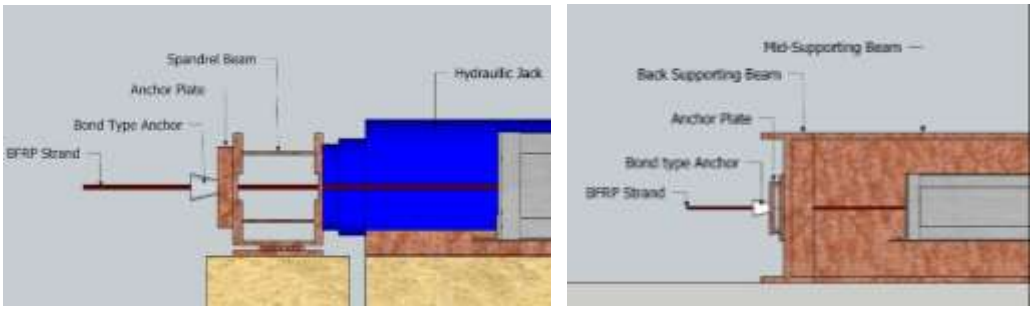

(b) Front Assembly (c) Back Assembly

Fig. 1. Pictorial Representation of the Experimental test Setup

The BFRP strands would be pretensioned using a 500 kN hydraulic jack by pushing the spandrel beam with a force of 65 kN, in order to create an initial prestress 0.50 f_{pu} in each strand. The bottom of the spandrel beam would be rested on 8 mm diameter mild steel bars to reduce the contact friction and allow the free movement of spandrel beam during the pre-tensioning operation (Fig. 1b). Thereafter, both the concrete beams would be cast and prestress would be transferred to the beams by releasing the

hydraulic jack after concrete reaches 70% of its mean characteristic compressive strength (f_{ck}). The load and strain in the BFRP strands would be measured immediately before and after the transfer of prestress.

4. Finite Element Analysis.

A three dimensional finite element model of the test setup has been developed using FE tool ABAQUS (2013) in order to perform the prestressing operations in accordance with the design principle explained above. Configuration details of the test setup has been designed by conducting a number of parametric studies on the developed model. Several parameters like the size and location of stiffener plates to be used and orientation of the sections have been thoroughly investigated.

4.1. Setting up the Analysis

The analysis procedure in ABAQUS (2013) consisted of five different steps. The first step represents the application of gravity loads in which the self-weight of all components of the test setup has been defined. The second step represents the jacking of the prestressing strands in which the BFRP strands have been tensioned by giving a displacement to the spandrel beam. The magnitude of the displacement has been defined based on the strand force generated during tensioning. In this step, the distribution of stresses along the length of strand remains constant and equal to the initial prestress (f_{si}). The third step represents the casting of concrete and the release of prestressing strand. Hence the bond stress between the strands and the surrounding concrete has been defined in this step. The release of the BFRP strands would be implemented by releasing the displacement given to the spandrel beam in the previous step. Since, the stresses in BFRP strands are within the elastic limit and the strands are locked at both the ends, the movement of the spandrel beam back to its original position would be restricted by the bond between strand and concrete. Thus the prestress force would be transferred to concrete. The fourth and fifth step represents the concrete shrinkage and creep causing a change in the stress profile in the pre-tensioned concrete member and prestressing strand. The various parts of the test setup and its nomenclature for the finite element analysis are shown in Table 2.

Table 2. Parts of the Base Line Setup

Members of the Test Setup	FE Model Nomenclature	Dimension/Length
ISMB 450-1	Back-Supporting Beam	1100 mm
ISMB-450-2	Mid-Supporting Beam	3000 mm
Built-up beam consisting of two ISMB-150 and 8mm thick Plates	Spandrel Beam	1100 mm
Back Supporting Beam Stiffeners	Stiffener Plate-1	400X70X12 mm
	Stiffener Plate-2	200X200X12 mm
Spandrel Beam Stiffeners	Stiffener Plate-3	180X150X20 mm
Anchors	BFRP Anchor	Length=50 mm
		Ext. Dia.=20mm, Int. Dia.=8mm
Concrete Beam	Concrete	200X100X3000 mm
BFRP Strand	Strand	Length=5000 mm, Dia.=8 mm

The FE model of the test setup has been meshed with eight nodded brick elements using structured mesh controls with the exception of the BFRP strands. The FE mesh of the BFRP strands has been refined using a sweep method with 16 divisions along the face with six nodded tetrahedral elements. This has resulted in a more uniform and refined mesh throughout the test setup as shown in Fig. 2.

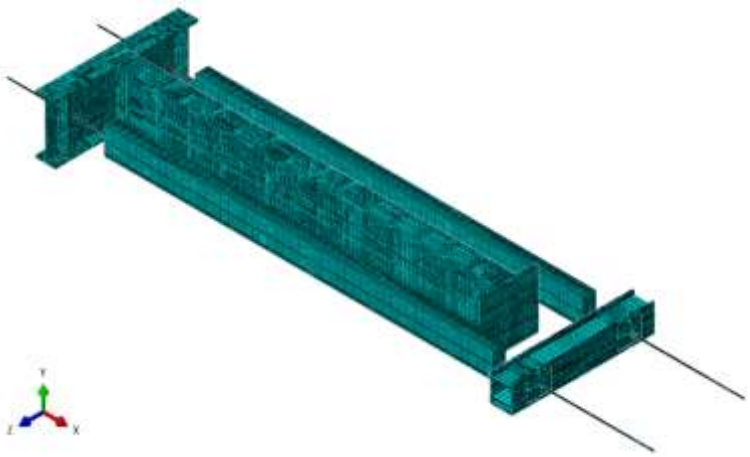

Fig. 2. Finite Element Assembly and Meshing

4.2. Input Parameters

The various parameters defining the constitutive relationship for materials, contact behavior, constraints, and appropriate boundary conditions such as displacement and/or force boundary conditions used to develop the FE model of the test setup are briefly explained in this section.

Constitutive Laws

BFRP Strands

The prestressing strand chosen for the present study is 8 mm diameter BFRP rebar commercially known as RockBar™ (Table 1). The strands are manufactured in circular cross-sections by Galen L.L.C., Russia. Each individual rod is made up of basalt fiber in an epoxy resin matrix and is sand blasted to increase its bond strength with concrete. In the present study a User Material (UMAT) code has been written to define the transversely isotropic linearly elastic material properties of the BFRP strands

Structural Steel

A quad-linear material model proposed by Yun and Gardner (2017) for FE-410 steel as shown in Fig. 3 has been utilized to accurately represent the elastic, yield plateau and strain hardening properties typically associated with hot-rolled steel sections.

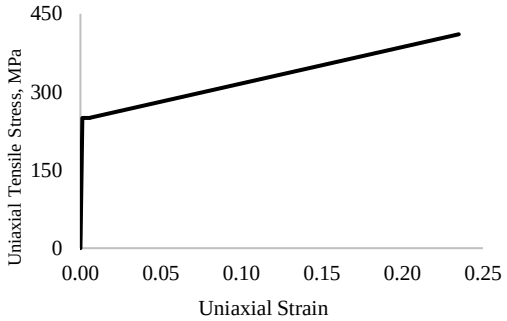

Fig. 3. Quad-Linear Stress-Strain model for Structural Steel Yun and Gardner (2017)

Concrete

The generalized compressive stress-strain relationship of concrete relating the uniaxial compressive stress (σ_c) to uniaxial compressive strain (ε_c) proposed by Tsai (1988). Eq. 1 has been utilized in the present study to model behaviour of concrete under compression. In Eq. 1, n and r are the parameters to control the slope of the curve and has been obtained for unconfined concrete from the model proposed by Mander et al. (1988).

$$\sigma_c = f'c\frac{nx}{1+\left(n-\frac{r}{r-1}\right)x+\frac{x^r}{r-1}} \quad (1)$$

Where,

$$x=\frac{\varepsilon_c}{\varepsilon'_c}, n=\frac{7.2}{f'^{3/8}_c}, r=\frac{f'_t}{5.2}-1.9$$

4.2.1. Bond Stress Slip Relationship

The cohesive interaction between two surfaces has been simulated in ABAQUS (2013) by using cohesive surface based approach. ABAQUS Theory Manual (V. 2013) assumes linear traction-separation behaviour which relates normal and shear stresses to the normal and shear separations across the interface before the initiation of damage. The nominal traction stress vector, t consists of three components t_n, t_s and t_t, and the corresponding separation is denoted by δ_n, δ_s and δ_t, where n, s and t represent normal, shear and tangential direction, respectively. The traction separation matrix shown in Eq. 2 provides coupled behaviour between all components of the separation vector and traction vector.

$$t_m=\begin{bmatrix}t_n\\t_s\\t_t\end{bmatrix}=\begin{vmatrix}k_{nn} & k_{ns} & k_{nt}\\k_{ns} & k_{ss} & k_{st}\\k_{nt} & k_{st} & k_{tt}\end{vmatrix}\begin{bmatrix}\delta_n\\\delta_s\\\delta_t\end{bmatrix}=k_m\delta_m \quad (2)$$

By default, the normal and tangential stiffness components will not be coupled, as pure normal separation by itself does not give rise to cohesive forces in the shear directions, and pure shear slip with zero normal separation does not give rise to any cohesive forces in the normal direction. Thus, it was decided to use uncoupled traction separation law which requires defining only the diagonal terms of the traction separation matrix shown in Eq. 2. According to Gan (2000), the contact stiffness's k_{nn} and k_{tt} are obtained by approximation of the bond-slip relationship. The stiffness of the normal traction is taken as 100 times the stiffness of the shear traction as shown in Eq. 3.

$$k_{ss}=k_{tt}=\frac{\tau_{\max}}{s_1}\ \text{N/mm}^3$$
$$k_{nn}=100k_{ss}\ \text{N/mm}^3 \quad (3)$$

BFRP Strand and Concrete

For the present study, results from bond tests performed on RockBar™ by Gallen L.L.C. at the National Research Laboratory, Moscow State University (shown in Fig. 4) has been utilized to define the contact algorithm between BFRP strands and concrete. A peak bond stress of 18 MPa corresponding to slip of 0.2 mm has been reported for 8 mm BFRP strand and concrete on the basis of pull-out bond test on strands embedded in concrete. Using Eq. 3, bond stress coefficient values of 87 N/mm^3 for k_{ss} and k_{tt} and 8700 N/mm^3 for k_{nn} has been used to define the traction separation law between the strands and the concrete in ABAQUS.

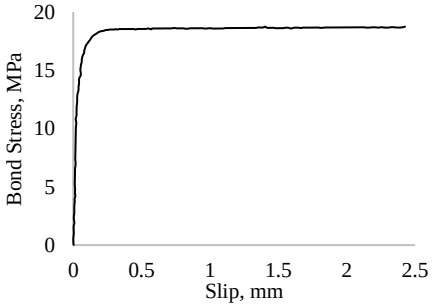

Fig. 4. Bond Stress Slip Relationship for RockRebar™

(Tested June 2017, Received on February, 2018 and Re-used with Permission from Mr. Egor Livinov, CMO, Galen L.L.C.)

BFRP Strand and Anchor

This study aims to develop a bond type anchor using steel tube and epoxy resin for holding the BFRP strands in the experimental setup. Since, the fixture is still under development, number of trial have been made in the FEA by increasing the contact stiffness's

between fixture and the strand. It has been observed that, if the contact stiffness is too low, the strand pulls out from the fixture and the analysis stops due to non-convergence error, whereas considering very high contact stiffness may be unrealistic to the actual experiment. Thus an optimum value of 60 N/mm^3 has been chosen as k_{ss} and k_{tt} to ensure convergence of the FE program for an initial prestress of 0.5 f_{pu}.

4.2.2. Concrete Creep and Shrinkage

It has been planned to perform time dependent studies by periodically measuring the increase in axial concrete strains with time due to creep and shrinkage over a period of 28 days after prestress release. The increase in axial concrete strains due to concrete creep and shrinkage will be periodically measured over a period of 28 days after prestress release. This increase in concrete strains have been incorporated in the FE model for the time dependent analysis as per guidelines obtained from IS 1343 (1984) and are shown in Table 3. In order to consider the aging of concrete with time, the modulus of elasticity of concrete has been defined as a Field Variable (FV) in the ABAQUS CAE environment. The variation of modulus of elasticity with time ($E_{cm}(t)$) has been estimated from the mean compressive strength at various time points $f_{cm}(t)$, using Eurocode BS EN 1992-1-1 (2004) guidelines as shown in Table 3. $E_{cm}(t)$ has been set to vary with the FV in the ABAQUS CAE environment to model the estimated variation in the property with time. An initial condition has been defined, to specify the initial value of FV for the set of concrete nodes. Then, a pre-defined field variable has been added in the first analysis step, representing prestress transfer in order to specify the value of FV as 1.0 for the same concrete node set. In further steps, the field variable has been changed from 2 to 4 indicating aging of concrete and increase in concrete elastic modulus. This has been done by editing the input file and then running the input file through ABAQUS (2013) command window. The Young's Modulus of concrete in the FE model will thus vary smoothly over the course of the steps as the FV value is ramped from 1.0 to 4.0 at all nodes in the concrete node set. The increase in concrete strains have been incorporated in the FE model by defining an equivalent differential temperature change (ΔT) in concrete using Eq. 4 at different step levels during the analysis. The calibration results for the FE model for time dependent analysis are shown in Table 3.

$$\Delta T = \frac{\varepsilon_t}{\alpha_c} \tag{4}$$

Where,

ε_t is the time dependent strain in concrete and α_c is the coefficient of thermal expansion of concrete.

Table 3. Calibration of FE Model for Time Dependent Analysis

Analysis Step	Filed Variable	Time (Days)	Concrete Properties [BS EN 1992-1-1 (2004)]			Increase in Concrete Strain	Temperature Input (ºC)
			$\beta_{cc}(t)$	f_{ck} (MPa)	E_c (MPa)		
Gravity	1				N.A.		
Initial Prestress	1				N.A		
Prestress Transfer	2	3	0.6629	26.52	28954.64	N.A.	0
Concrete Shrinkage	3	7	0.8187	32.75	29781.41	0.0003*	-20.69
Concrete Creep	4	28	1	40.00	31622.70	0.00018	-12.41

* A concrete shrinkage strain of 0.0003 has been considered before creep strain starts

4.2.3. Boundary Condition

Rotational and translational constraints along the Z direction has been applied throughout the length and width of the FE model of the test setup in order to simulate the resting condition of the setup on the ground and its symmetry about XY plane (refer to Fig. 2 for orientation of the X, Y and Z axes). Furthermore, a partial translational constraint along the Y direction has been applied in the FE model to restrain the movement of the test setup only in the downward direction.

5. Result and Discussion

5.1. Initial Prestress Results and Optimization of Members

FEA results have been used to ensure there is no damage to the setup during initial prestressing. Thus, the first two steps of the FEA were performed to ensure that the jacking of the BFRP strands up to a stress of 0.50 f_{pu} does not cause yielding of any component of the test-setup and does not generate additional torsional stresses or twisting in setup. The results obtained at the end

of the second step of the FEA have been utilized to check the functionality of the test setup as well as for material yielding. Hence each component of the test setup were checked to ensure there are no plastic strains when the stresses in the BFRP strands reached 643 MPa (0.50 f_{pu}). Based on the strain obtained in the various components of the test setup, the back supporting beam and the spandrel beam were found to exceed the yield condition defined in the FE model, as shown in Fig. 5. Hence the back supporting beam and the spandrel beam have been strengthened to avoid yielding of these components due to the initial stretching of the BFRP strands. The modifications made to strengthen these components are discussed in Sections 5.1.1 and 5.1.2.

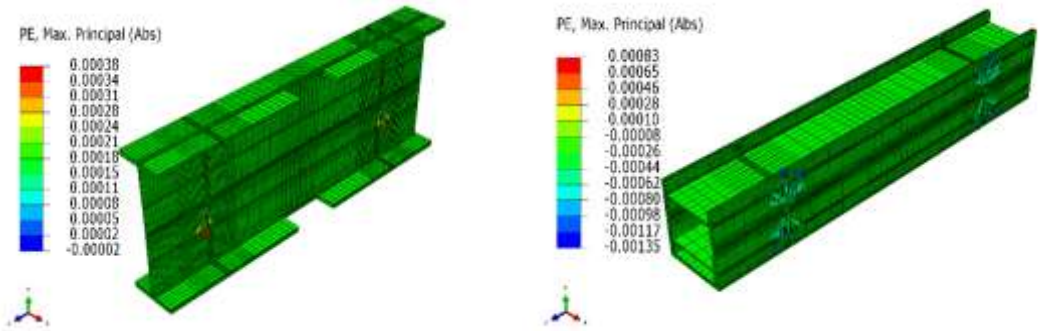

(a) Plastic Strains in Back Supporting Beam (b) Plastic Strains in Spandrel Beam.

Fig. 5. Results from Base Line Analysis of Experimental Test Setup

5.1.1. Stiffening of Back Supporting Beam

Two additional vertical stiffener plates of dimensions 415 mm X 70 mm X 12 mm were added and extending from the top flange to the bottom flange of the I-section in order to avoid the yielding of the back supporting beam. Additionally, 2 horizontal stiffener plates of dimension 200 mm X 200 mm X 12 mm have been added at the hole location of the back supporting beam, as shown in Fig. 6a. The FEA of the model with the stiffened back supporting beam has been performed with the same initial stress in the BFRP strands and to ensure plastic strains don't develop in the strengthened back supporting beam. The increase of Von Mises stress at the previously yielded location of the back supporting beam has been plotted with the increasing axial stress in the strand as shown in Fig. 6b. It can be observed, for the same axial stress in strand, the Von Mises in the back supporting beam does not reach the yield condition due to the addition of stiffener plates.

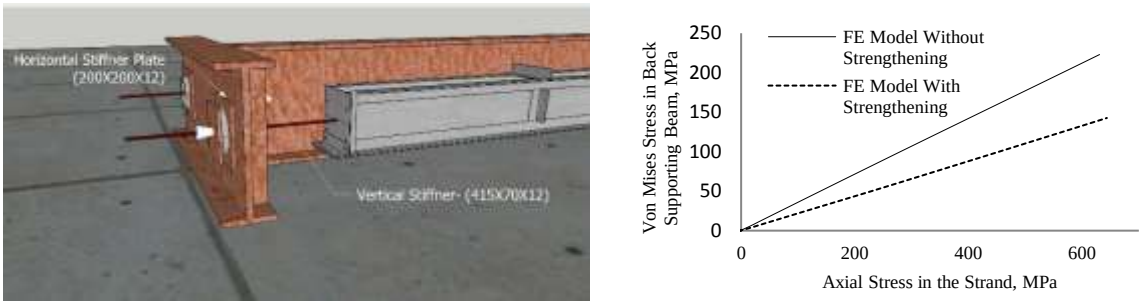

(a) Location and Dimensions of Stiffener Plates (b) FE Result after adding Stiffener Plates

Fig. 6. Optimization of Back Supporting I Beam

5.1.2. Stiffening of Back Spandrel Beam

In order to eliminate the plastic strains observed in the spandrel beam, two stiffener plates of dimension 180 mm X 150 mm X 20 mm have been attached to the spandrel beam at the hole locations (Fig. 7a). The increase of Von Mises stress at the previously

yielded location of the spandrel beam has been plotted with the increase of stress in the strand as shown in Fig. 7b. Once again it can be observed from Fig. 7b that the addition of the stiffener plates delayed the yielding of the spandrel beam significantly.

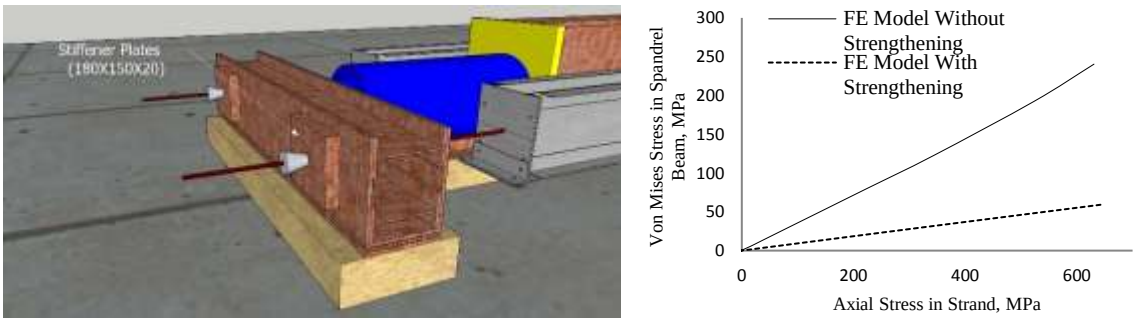

(a) Location and Dimensions of Stiffener Plates (b) FE Result after adding Stiffener Plates

Fig. 7 Optimization of Spandrel Beam Prestress Transfer.

5.2. Prestress Transfer

The release of the prestressing jack creates radial stress and activates a frictional resistance between the concrete and the strand which enhances the transfer of prestress force in to the concrete until the stress in strand just outside the concrete beam becomes zero (Fig. 8a). The stress in strand changes from initial prestress (f_{si}) of 643 MPa to effective prestress (f_{se}) of 639 MPa at the central length of the concrete beam indicating a prestress loss of 4 MPa due to elastic shortening of concrete member, as shown in Fig. 8b.

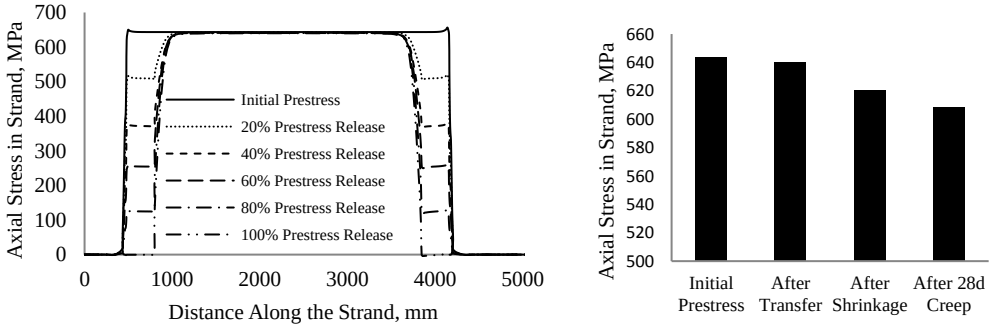

(a) Variation of Stress in Strand during Prestress Transfer (b) Variation of Effective Prestress in Strand

Fig. 8. Strand Stress Variation during Prestress Transfer

5.3. Concrete Cracking along the Transmission Length

FEA results showed significant amount of plastic strains in concrete around or near the prestressing strands (Fig. 9) which indicates concrete cracking in these regions during prestressing operations. These cracks are caused primarily by the concentration of prestressing forces at the time of prestress release.

In order to control the stress concentration at the end of pretensioned members and avoid cracking, several researchers deliberately debonded selected strands with concrete at and near anchorage zones. However, for better prediction of the state of stress and the nature of damage in the critical regions of concrete beams pretensioned with BFRP strands, this study focuses on determining the state of stress in the end-zone of prestressed concrete beams without debonding the strands at the end region so that more effective steps can be taken in the design to control such cracking.

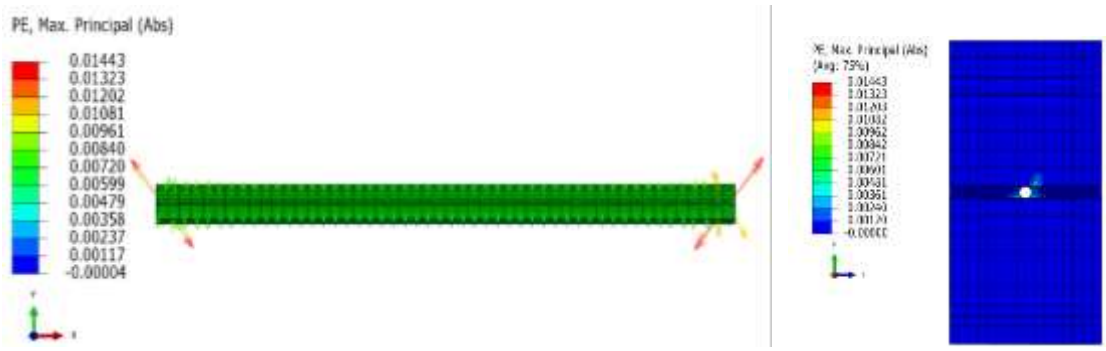

(a) Plastic Strains along the Length of Beam (b) Plastic Strains along the Cross-Section

Fig. 9 Plastic Strain in Concrete Beam during Prestress Transfer

5.4. Transmission Length

In the present study, the transfer length of the strands has been predicted by plotting the stress profile along the strand and along the concrete surface (Fig. 10a and 10b) and measuring the transfer length at 95% of the Absolute Maximum Stress (95% AMS) as recommended by Russell and Burns (1993). In case of actual experiments, these reading are generally recorded using Electrical Resistance Strain Gauge (ERSG) pasted along the strand and concrete surface. However, the ERSGs utilized for measuring transfer length through strand has been proved to be unreliable for several reasons. First of all, relative displacements between strand and concrete can destroy the strain gauge mounted on the strand. Secondly, the presence of ERSGs on the strand interferes with bond locally. The adverse effect of too many ERSGs mounted on a strand would affect the test result. Lastly, the gauges are difficult to protect during casting and are susceptible to damage from vibrators or damage by moisture during casting of concrete. All of these factors compound to render ERSGs ineffective in measuring transfer length of pretensioned strand.

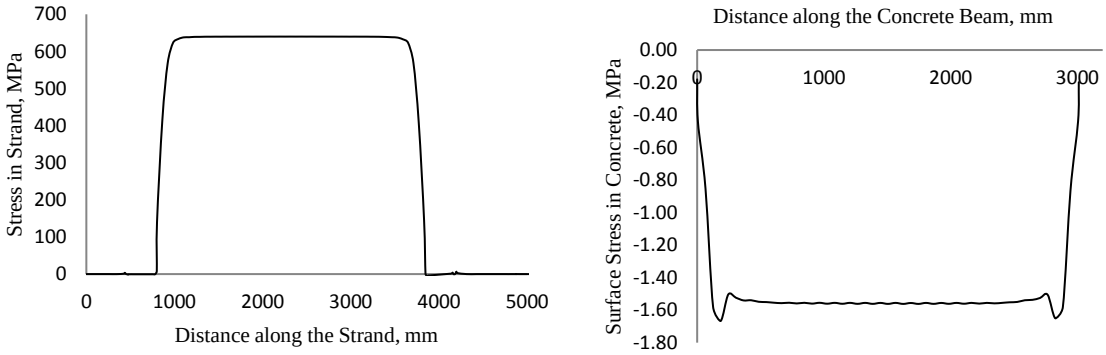

(a) Stress Profile along the Strand (b) Stress Profile along Concrete Surface

Fig. 10 Variation of Stress Profile to Measure Transfer Length

Measurement of the strains on the outside surface of the concrete has proved to be the most reliable technique to measure the transfer length [Russell and Burns (1993)]. Using this FE study it has been found that the transfer lengths obtained by directly measuring strains on the strand during transfer and by measuring strain on concrete surface at the strand location, are both equal to 167 mm i.e. $20\,d_b$ for BFRP strands.

5.5. End Slip

The difference between the steel and concrete strains creates a relative movement of the strand with respect to the surrounding concrete and commonly results in end slips of the strands. The end slip has been obtained directly from the FE model as the relative movement between strand and concrete at the end of prestressing step, as shown in Fig. 11. The initial elongation of the strand has

been subtracted from the strand retraction after prestress release to obtain the net displacement of the strand. The concrete shortening has been further subtracted from the net displacement of the strand to get a net end slip of 0.36 mm.

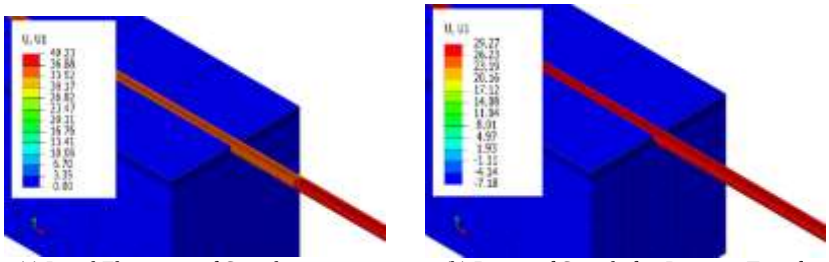

(a) Initial Elongation of Strand (b) Return of Strand after Prestress Transfer

Fig. 11 Pictorial Representation of Strand Movement before and after Prestress Transfer

5.6. Time Dependent Result

It can be observed from Fig. 12 that the increase in concrete strains due to shrinkage and creep results in reduction of effective prestress. A total stress loss of 31 MPa has been observed after 28 days due to the combined effect of concrete shrinkage and creep. Note that the relaxation loss of BFRP strand has been neglected in the present simulation due to insufficient data available on the creep behaviour of BFRP strands. Therefore the actual loss in the experiment may be slightly higher than the FE prediction.

The transfer length, determined from changed strain profiles in the strand indicate that there is no significantly change in the transfer length of BFRP strands since the time of release. This observations could be due to smaller dimension of concrete member and a shorter duration (28 days) over which the analysis has been performed. This observation needs to be re-evaluated and corroborated through further experimental research by observing the strains over a longer duration.

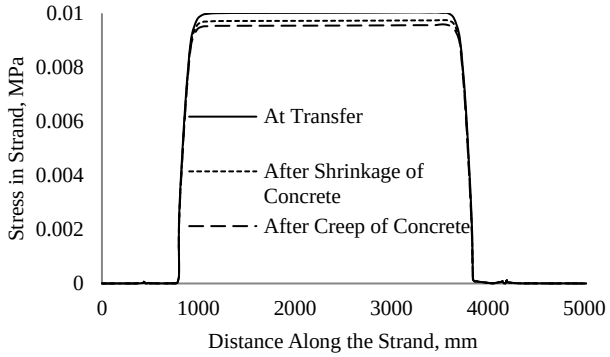

Fig. 12. Time Dependent Strain Variation in Strand

6. Summary and Conclusion

Nonlinear FEA has been performed prior to fabrication to validate the design and optimisation of the test setup dimensions. Based on the extensive FEA following conclusion has been drawn:

- The modelling process meticulously reflects all the experimental conditions beginning with strand tensioning operation, stress transfer and time dependent behaviour.
- From the finite element study, a robust experimental test setup capable of stressing and releasing BFRP strands has been established.
- Based on the FE results, a transfer length of 167 mm ($20\,d_b$) and an end slip of 0.36 mm has been predicted for BFRP strands.
- Results for time dependent FE analysis did not show significant increase in transfer length over a period of 28 days

References

ACI 440R-96, 1996, State of the Art Report on Fiber Reinforced Plastic (FRP) Reinforcement for Concrete Structures, American Concrete Institute, Farmington Hills, MI, USA.

ABAQUS, 2013. ABAQUS Software Version, 6.13, Dassault Systèmes Simulia Corp Providence RI, USA.

ABAQUS Theory Manual, 2013. ABAQUS Analysis User's Manual Version, Dassault Systèmes Simulia Corp Providence RI, USA.

Atutis, M., Valivonis, J., Atutis, E., 2018. Experimental Study of Concrete Beams Prestressed With Basalt Fiber Reinforced Polymers. Part II: Stress Relaxation Phenomenon, Composite Structures. V. 144, pp 114-123.

Belarbi, A., Dawood, M., Mirmiran, A., Bowman, M., 2017. Synthesis of Concrete Bridge Piles Prestressed with CFRP Systems, Department of Civil and Environmental Engineering. University of Houston, Houston, TX, USA.

Colajanni, P., Recupero, A., Ricciardi, G., Spinella, N., 2016. Failure by Corrosion in PC Bridges: A Case History of a Viaduct in Italy, International Journal of Structural Integrity. V. 7, N. 2, pp.181-193.

Economic Times, 2016. India Loses up to $100 Billion Annually to Corrosion: Hind Zinc CEO Sunil Duggal, Retrieved from http://www.economictimes.com.

Eurocode, BS EN 1992-1-1, 2004. Design of Concrete Structures-Part 1-1: General Rules and Rules for Buildings, British Standards. Comité Européen de Normalisation.

Gamble, L., Fadl, I., Gregg, W., Jenny, D., Mallett, J., Tadros, M., Ghali, A.,Workman E., 1976. Recommendations for Estimating Prestress Losses, PCI Journal, Precast/Prestressed Concrete Institute. Chicago, IL. V. 21, N. 2, pp. 108-26.

Gan, Y., 2000. Bond Stress and Slip Modelling in Nonlinear Finite Element Analysis of Reinforced Concrete Structures. PhD Thesis, University of Toronto, Toronto, ON, Canada.

IS 1343 1984, Indian Standard Code of Practice 1343. 1984. Code of Practice for Prestressed Concrete. Bureau of Indian Standards, New Delhi, Delhi.

Mander, B., Priestley, J., Park, R. 1988. Theoretical Stress-Strain Model for Confined Concrete, ASCE Journal of Structural Engineering. V. 114, N. 8, pp 1804-1826.

Russell, W., and Burns, H., 1993. Design Guidelines for Transfer, Development and Debonding of Large Diameter Seven Wire Strands in Pretensioned Concrete Girders, Final report. No. FHWA/TX-93+ 1210-5F.

Poston, R. and West S., 2005. Investigation of the Charlotte Motor Speedway Bridge Collapse, In Structures Congress, Metropolis and Beyond. pp. 1-11.

Shi, J., Wang, X., Wu, Z., Zhu, Z., 2015. Relaxation Behaviour of BFRP Tendon for Prestressing Application, International Conference on Performance-based and Life-cycle Structural Engineering, Brisbane, Australia. pp. 434-442.

Saadatmanesh, H., Tannous, E., 1999. Relaxation, Creep, and Fatigue Behavior of Carbon Fiber Reinforced Plastic Tendons. ACI Materials Journal. V. 96, N. 2, pp 143-53.

Saadatmanesh, H., Tannous, E., 1999. Long-term Behavior of Aramid Fiber Reinforced Plastic (AFRP) Tendons. ACI Materials Journal. V. 96, N. 2, pp 297-305.

Tsai, T., 1988. Uniaxial Compressional Stress-Strain Relation of Concrete, ASCE Journal of Structural Engineering. V. 114, N. 9, pp 2133-2136.

Thorhallsson, R., Gudmundsson, H., 2013. Test of Prestressed Basalt FRP Concrete Beams With and Without External Stirrups, International Proceedings of Fib Symposium Engineering a Concrete Future: Technology. Mmodelling & Construction. pp 393-396.

Younes, T., Mayah, A., Topper T, 2017. Fatigue Performance of Prestressed Concrete Beams using BFRP Bars, Construction and Building Materials. V. 157, pp 313-21.

Yun, X., Gardner, L., 2017. Stress-Strain Curves for Hot-Rolled Steels. Journal of Constructional Steel Research. V. 133, pp 36-46.

Wu, Z., Wang, X., Wu, G., 2009. Basalt FRP Composite as Reinforcements in Infrastructure, International Proceedings, 17th Annual International Conference on Nano Engineering. New Orleans, USA. pp. 21-24.